Supplementary Material

1 Samples and reference regions

Supplementary Table 1. Investigated loess sequences, number of analysed samples and sampling resolutions used in this study.

Region	LPS	Coordinates and elevation	No. of samples	Sampling resolution [cm]	Reference
Lower Danube Basin	Urluia	44°06‘ N 27°54‘ E 125 m a.s.l.	425	2	Obreht et al. (2017)
	Rasova	44°15’ N 27°57’ E 28 m a.s.l.	350	2	Zeeden et al. (2018)
	Vlasca	44°24’ N 27°52’ E 37 m a.s.l.	625	2	Obreht et al. (2017)
	Sageata	45°06’ N 26° 58’ E 65 m a.s.l.	52	10	this study
	Balta Alba Kurgan	45°17’ N 27°17’ E 46 m a.s.l.	550	2	this study
Lower Austria	Langenlois	48°28’ N	201	4	this study

		15°41’ E 232 m a.s.l.			
Central Hungary	Ságvár	46°49’ N 18°6’ E 181 m a.s.l.	97	5	Bösken et al. (2018)
Northeast Hungary	Bordrogkeresztúr	48°09’ N 21°22’ E 105 m a.s.l.	83	4	Bösken et al. (2019)
Vojvodina	Orlovat	45°15’ N 20°35’ E 88 m a.s.l.	93	4	Obreht et al. (2015)
	Petrovaradin	45°16’ N 19°51’ E	34	5	Marković et al., (accepted)
	Irig	45°05’ N 19°52‘ E 94 m a.s.l.	60	10	Marković et al. (2007), Pötter et al. (accepted)
Southern Ukraine	Kurortne	45°54’ N 30°16’ E 15 m a.s.l.	145	3	Tecsa et al. (2020)

2 Geochemical compositions of the investigated loess-palaeosol sequences

Supplementary Table 2. Minimum, maximum and mean values for major and trace element composition for the investigated LPS and the reference regions: URL: Urluia; RAS: Rasova; VLA: Vlasca: SAG: Sageata; BAK: Balta Alba Kurgan (all Lower Danube Basin, Romania); LLS: Langenlois (Lower Austria); SAV: Ságvár (Lake Balaton, Central Hungary); BKT: Bodrogkeresztúr (Bükk Mountains, North-eastern Hungary); ORL: Orlovat, PET: Petrovaradin; IRI: Irig (all Vojvodina) and KUR: Kurortne (Black Sea, Ukraine).

Element [unit]		**URL** *Lower Danube Basin*	**RAS** *Lower Danube Basin*	**VLA** *Lower Danube Basin*	**SAG** *Lower Danube Basin*	**BAK** *Lower Danube Basin*	**LLS** *Lower Austria*	**SAV** *Northern Hungary*	**BKT** *Northern Hungary*	**ORL** *Vojvodina*	**PET** *Vojvodina*	**IRI** *Vojvodina*	**KUR** *Black Sea Shore*
Na_2O [%]	min	0.73	0.81	0.76	0.73	0.67	0.75	0.71	0.78	0.73	0.84	0.71	0.54
	max	1.18	2.14	1.22	4.84	1.52	1.08	1.23	1.43	1.28	1.11	1.28	0.72
	mean	0.92	1.00	1.00	1.34	1.00	0.89	0.85	1.10	0.94	0.96	0.94	0.63
Al_2O_3 [%]	min	8.67	9.20	8.98	8.72	8.91	7.33	8.02	10.16	9.48	9.58	8.52	7.82
	max	12.17	12.94	12.65	17.06	14.95	11.26	11.24	14.58	15.09	12.68	13.24	12.66
	mean	10.28	10.68	10.46	12.01	10.86	9.28	8.93	12.68	11.02	10.77	10.83	10.36
SiO_2 [%]	min	35.68	39.11	42.06	41.51	39.84	35.34	35.98	42.43	38.48	35.65	34.56	43.00
	max	52.24	52.80	54.10	60.41	66.72	42.8	52.61	62.92	54.14	46.45	51.83	62.65
	mean	43.36	45.61	48.73	52.78	50.41	39.29	42.15	57.58	43.20	39.88	42.46	52.34
K_2O [%]	min	1.38	1.44	1.52	1.70	1.55	1.12	1.24	1.38	1.10	1.70	1.32	1.63
	max	2.01	3.01	2.07	6.01	2.32	1.80	1.59	2.50	2.31	2.34	2.02	2.38

	mean	1.68	1.75	1.74	2.71	1.89	1.48	1.38	2.00	1.79	1.97	1.68	1.95
TiO_2 [%]	min	0.67	0.70	0.69	0.48	0.63	0.60	0.60	0.75	0.42	0.66	0.63	0.64
	max	0.92	1.00	0.91	0.84	0.90	0.84	0.76	1.00	0.83	0.81	0.87	0.86
	mean	0.78	0.83	0.79	0.68	0.74	0.71	0.68	0.88	0.77	0.72	0.75	0.75
Fe_2O_3 [%]	min	3.62	3.90	1.91	3.39	3.49	2.98	1.92	3.67	2.83	3.89	3.50	2.67
	max	4.62	4.85	4.64	5.17	4.70	4.59	3.69	5.00	4.76	4.91	5.42	4.27
	mean	4.12	4.21	4.05	4.15	4.16	3.65	3.26	4.53	4.34	4.29	4.44	3.66
V [mg/kg]	min	69	72	69	44	73	55	50	63	43	83	71	58
	max	110	118	109	119	118	99	98	114	118	112	122	106
	mean	90	91	93	92	95	75	65	93	94	96	96	89
Cr [mg/kg]	min	73	78	73	3	71	54	61	82	54	66	63	61
	max	382	265	131	53	106	79	297	229	125	104	113	102
	mean	102	127	92	37	85	67	88	110	95	79	88	81
Ni [mg/kg]	min	30	29	30	71	30	19	21	30	34	31	28	19
	max	44	46	45	307	46	35	38	46	50	42	54	38
	mean	37	38	36	115	37	25	25	39	42	36	42	30
Rb [mg/kg]	min	60	59	64	94	63	55	34	69	51	70	62	64
	max	85	46	91	374	87	86	70	101	88	94	99	93
	mean	71	38	76	198	75	69	59	83	77	81	81	78

Sr [mg/kg]	min	113	132	136	94	86	165	106	92	104	143	102	92
	max	258	203	233	374	251	203	214	128	217	241	207	226
	mean	190	167	161	198	177	187	176	109	173	189	165	151
Y [mg/kg]	min	24	27	25	21	24	24	17	26	20	25	24	23
	max	35	41	34	41	34	39	32	37	35	32	34	32
	mean	29	32	30	28	28	29	27	32	30	28	30	28
Zr [mg/kg]	min	291	330	331	294	325	274	349	310	311	281	282	401
	max	495	715	461	594	569	507	748	571	1,725	355	394	562
	mean	368	463	386	391	407	368	419	433	398	313	333	472
Ba [mg/kg]	min	275	250	286	238	313	211	208	299	227	296	262	306
	max	377	437	536	474	447	406	313	450	283	374	408	402
	mean	322	321	343	359	381	277	247	359	333	333	342	358
Th [mg/kg]	min	9	11	10	9	9	10	7	10	9	11	10	9
	max	15	24	15	43	14	16	12	15	14	14	15	13
	mean	12	13	12	15	11	13	11	13	12	12	13	11

Supplementary Table 2. Provenance studies in the study area and reference regions.

Region	LPS	Methods	Potential main source areas	Reference
Lower Austria	Krems-Wachtberg, Stratzing, Wels	Trace element (Cr, Nb, Zr) geochemistry and U-Pb geochronology on detrital rutile grains	Danube alluvium, river sediments from Eastern Alps (Wels)	Újvári et al. (2013)
	Krems-Wachtberg, Stratzing, Wels	Cathodoluminescence, Hf isotope geochemistry and U-Pb geochronology on zircons	Local source rocks for heavy minerals	Újvári & Klötzli (2015)
Central Hungary	Süttő	XRF scanning, XRD mineralogy	Danube alluvium, local sources	Profe et al. (2018)
	>80 sampling sites in Hungary	Heavy mineralogy	Danube alluvium, reworked Cenozoic sands	Thamó-Boszó et al. (2014)
	Majs, Nagynyárád, Tötös	Geochemistry (XRF)	Danube alluvium	Újvári et al. (2008)
	Mende, Paks, Zmajevac (HR), Basaharc, Baltavár, Danitz-puszta, Mohács, Dunaszekcső	Clay mineralogy (XRD), Sr-Nd isotopes, zircon U-Pb geochronology	Danube alluvium, exposed local rocks	Újvári et al. (2012)
Northeastern Hungary	Tokaj	Geochemistry (XRF and Sr-Nd isotopes)	Tisa alluvium, West and East Carpathians, Miocene sands	Schatz et al. (2015b)

Vojvodina	Orlovat	Geochemistry (XRF)	Danube alluvium, Tisa alluvium, tributaries, Deliblato Sands	Obreht et al. (2015)
	Batajnica/Stari Slankamen	Geochemistry (XRF)	Danube alluvium, Tisa alluvium	Buggle et al. (2008)
Lower Danube Basin	Mircea Voda	Geochemistry (XRF)	Danube alluvium, aeolian sands	Buggle et al. (2008)
Ukraine	Stary Kaydaky	Geochemistry (XRF)	Glaciofluvial outwash plains	Buggle et al. (2008)
	18 outcrops in Poland and Ukraine	Zircon U-Pb geochronology	Dniester alluvium, tributaries (Poland, W.-Ukraine); glaciofluvial outwash plains (C.-Ukraine)	Pańczyk et al. (2020)
	Roxolany	U-Pb geochronology of zircons, Anisotropy of magnetic susceptibility	Dniester alluvium	Nawrocki et al. (2018)

Supplementary Table 3. Wind direction studies in the study area and reference regions.

Region	Sites	Methods	Palaeowind directions	Reference
Lower Austria	Ventifacts in Eastern Austria, aeolian sands in Bohemian Massif	Geomorphological evidence; luminescence dating of sand deposits	W-NW	Sebe et al. (2015)
Central Hungary	Mega yardang system	Geomorphological evidence	NW	Sebe et al. (2011)
	Ventifacts	Geomorphological evidence	NW	Sebe (2013)
	LPS Bag, Basaharc, Dunaszekcsodblac, Galgahéviz, Hévízgyörk, Isaszeg, Siógarád	Anisotropy of magnetic susceptibility	NNW-NNW	Bradák (2009)
Vojvodina	LPS Bansko Brdo Hill (HR)	Scanning electron microscopical analysis, geographical evidence	N-NW	Banak et al. (2013)
	Deliblato Sands	Geomorphological evidence, Anisotropy of magnetic susceptibility	NW, strong component of local Košava wind (SE)	Gavrilov et al. (2018)
Lower Danube Basin	Gredas in the eastern Foreland of the Carpathians	Geomorphological evidence	NW-N	Rozycki (1967)
Ukraine	LPS in Poland and Ukraine	Endmember modelling of grain size distributions	W-NW	Bokhorst et al. (2011)

3 Age model

The age model used in this includes published age models from the investigated loess-palaeosol sequences, which are based on luminescence dating, radio carbon dating and (palaeo-) magnetic correlation techniques, as well as tephrochonological evidence (Obreht et al., 2017; Zeeden et al., 2018, Scheidt et al., this issue). The established tie points from these publications were extracted harmonized to establish a comparable age range and to obtain an age model on a marine isotope stage (MIS) scale. Since only the age model for URL covers the time span of interest (MIS 3 to 1), the age models for VLA and BAK had to be expanded. The chosen starting point was MIS 3, which is correlated to moisture enhancement and enhanced pedogenesis in south-eastern Europe (Zeeden et al., 2016). Therefore the starting point was set to the beginning of the enhancement of proxies for sediment moisture and pedogenesis, namely magnetic susceptibility (MS; Fig. S1) and clay content (CC; Fig. 7). Additionally, the data was visually compared to $\delta^{18}O$ data from the NGIRP ice core (North Greenland Ice Core Project members, 2004). For URL, this is in a depth of 8.5 m, for VLA in 12.5 m and in BAK in 10.9 m. The Campanian Ignimbrite (CI) tephra was used as a marker horizon for all sequences. The onset of MIS 2 was defined by the beginning of dry and cold conditions, namely where the lowest values of MS and CC are reached. In URL, the depth correlated to the onset of MIS 2 is 4 m, for RAS 4.5 m, for VLA its 7 m, 3.5 m for SAG and for BAK 6.2 m. The onset of MIS 1 was placed near the lower boundary of the Holocene soil formation.

4 Supplementary Figures

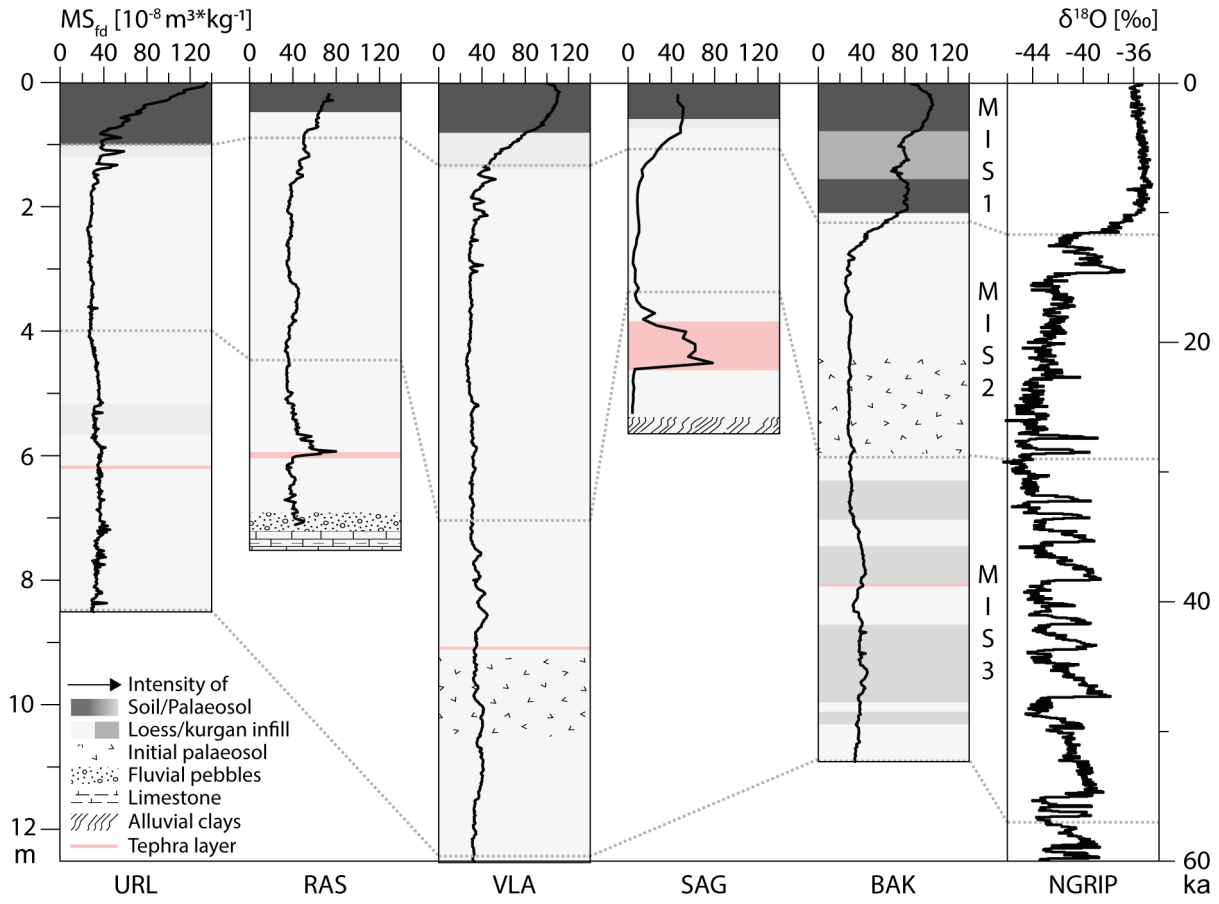

Supplementary Figure 1. Correlative age model for the LPS in the Lower Danube Basin, based on published age models and correlation of magnetic susceptibility data for the investigated loess-palaeosol sequences, sorted from south to north (URL: Urluia; RAS: Rasova; VLA: Vlasca; SAG: Sageata, BAK: Balta Alba Kurgan). $\delta^{18}O$ data from the NGRIP ice core in Greenland adapted from North Greenland Ice Core Project members (2004).

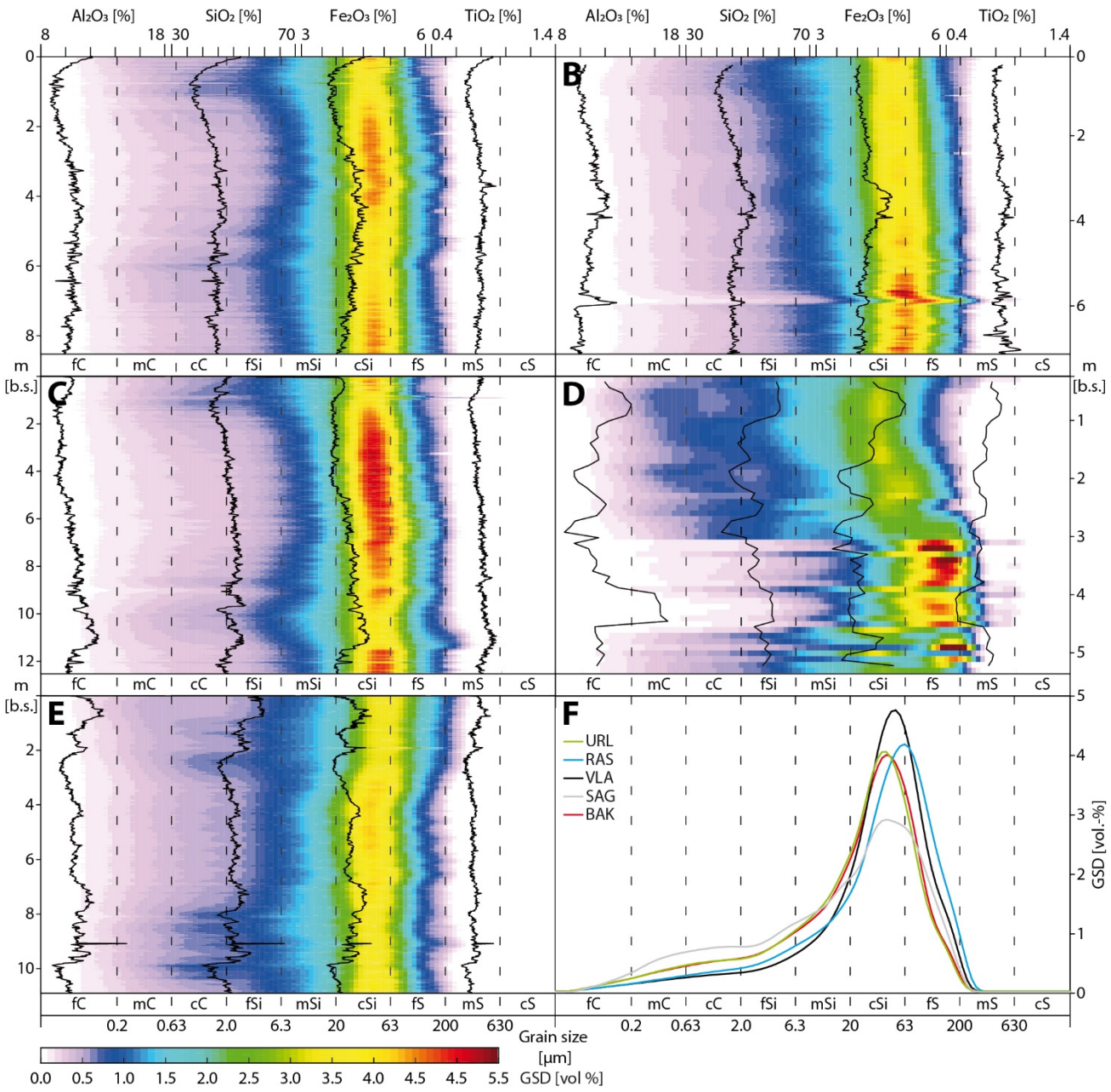

Supplementary Figure 2. Grain size distributions for the investigated sections, sorted from south to north (A: Urluia; B: Rasova; C: Vlasca; D: Sageata, E: Balta Alba Kurgan). F: Grain size distributions for unweathered loess from the investigated sections (URL: Urluia; RAS: Rasova; VLA: Vlasca; SAG: Sageta; BAK: Balta Alba Kurgan). Contents of chosen major element concentrations are shown as depth plots.

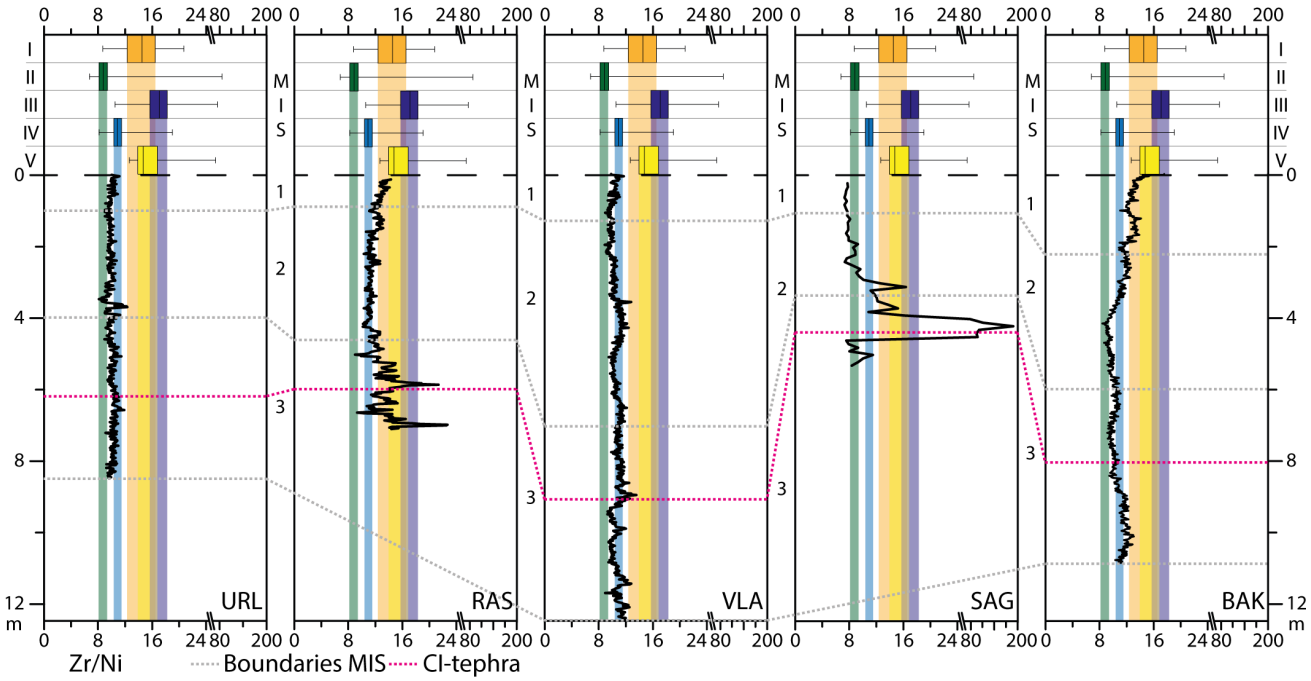

Supplementary Figure 3. Depth variations of the Zr/Ni ratios for the investigated loess-palaeosol sequences, sorted from south to north (URL: Urluia; RAS: Rasova; VLA: Vlasca; SAG: Sageata, BAK: Balta Alba Kurgan). The box-whisker plots on top show the composition of the sections from the reference regions: I: Lower Austria; II: Vojvodina; III: Balaton (Central Hungary); IV: Bükk Mountains (Northeast Hungary) and V: Black Sea Shore (Ukraine). The interquartile area (between 25% and 75% quartile) are shown as shaded boxes. The correlative age model as well as the CI-tephra are shown for temporal comparison.

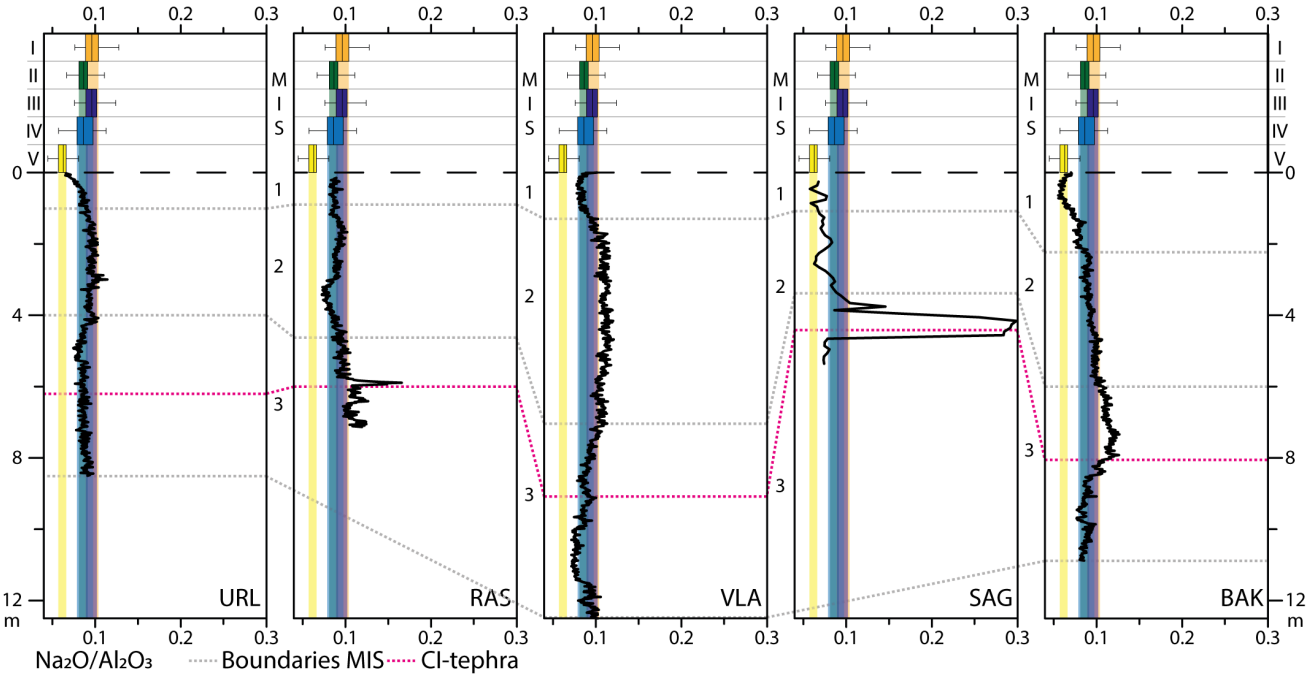

Supplementary Figure 4. Depth variations of the Na_2O/Al_2O_3 ratios for the investigated loess-

palaeosol sequences, sorted from south to north (URL: Urluia; RAS: Rasova; VLA: Vlasca; SAG: Sageata, BAK: Balta Alba Kurgan). The box-whisker plots on top show the composition of the sections from the reference regions: I: Lower Austria; II: Vojvodina; III: Balaton (Central Hungary); IV: Bükk Mountains (Northeast Hungary) and V: Black Sea Shore (Ukraine). The interquartile area (between 25% and 75% quartile) are shown as shaded boxes. The correlative age model as well as the CI-tephra are shown for temporal comparison

5 References

Bösken, J., Obreht, I., Zeeden, C., Klasen, N., Hambach, U., Sümegi, P., et al. (2019). High-resolution paleoclimatic proxy data from the MIS3/2 transition recorded in northeastern Hungarian loess. *Quat. Int.* 502, 95–107. doi:10.1016/j.quaint.2017.12.008.

Bösken, J., Sümegi, P., Zeeden, C., Klasen, N., Gulyás, S., and Lehmkuhl, F. (2018). Investigating the last glacial Gravettian site 'Ságvár Lyukas Hill' (Hungary) and its paleoenvironmental and geochronological context using a multi-proxy approach. *Palaeogeogr. Palaeoclimatol. Palaeoecol.* 509, 77–90. doi:10.1016/j.palaeo.2017.08.010.

Marković, S. B., Oches, E. A., McCoy, W. D., Frechen, M., and Gaudenyi, T. (2007). Malacological and sedimentological evidence for "warm" glacial climate from the Irig loess sequence, Vojvodina, Serbia. *Geochem. Geophys. Geosystems* 8, Q09008. doi:10.1029/2006GC001565.

Marković, S. B., Vandenberghe, J., Stevens, T., Mihailović, D., Gavrilov, M. B., Radaković, M. G., et al. (accepted). Geomorphological evolution of the Petrovaradin Fortress Paleolithic site (Novi Sad, Serbia). *Quat. Res.*

North Greenland Ice Core Project members (2004). High-resolution record of Northern Hemisphere climate extending into the last interglacial period. *Nature* 431, 147–151. doi:10.1038/nature02805.

Obreht, I., Hambach, U., Veres, D., Zeeden, C., Bösken, J., Stevens, T., et al. (2017). Shift of large-scale atmospheric systems over Europe during late MIS 3 and implications for Modern Human dispersal. *Sci. Rep.* 7, 5848. doi:10.1038/s41598-017-06285-x.

Obreht, I., Zeeden, C., Schulte, P., Hambach, U., Eckmeier, E., Timar-Gabor, A., et al. (2015). Aeolian dynamics at the Orlovat loess–paleosol sequence, northern Serbia, based on detailed textural and geochemical evidence. *Aeolian Res.* 18, 69–81. doi:10.1016/j.aeolia.2015.06.004.

Pötter, S., Schmitz, A., Lücke, A., Schulte, P., Obreht, I., Zech, M., et al. (accepted). Middle to Late Pleistocene environments based on stableorganic carbon and nitrogen isotopes of loess-palaeosolsequences from the Carpathian Basin. *Boreas*.

Tecsa, V., Gerasimenko, N., Veres, D., Hambach, U., Lehmkuhl, F., Schulte, P., et al. (2020). Revisiting the chronostratigraphy of Late Pleistocene loess-paleosol sequences in southwestern Ukraine: OSL dating of Kurortne section. *Quat. Int.* 542, 65–79. doi:10.1016/j.quaint.2020.03.001.

Zeeden, C., Hambach, U., Veres, D., Fitzsimmons, K., Obreht, I., Bösken, J., et al. (2018). Millennial scale climate oscillations recorded in the Lower Danube loess over the last glacial period. *Palaeogeogr. Palaeoclimatol. Palaeoecol.* 509, 164–181. doi:10.1016/j.palaeo.2016.12.029.

Zeeden, C., Kels, H., Hambach, U., Schulte, P., Protze, J., Eckmeier, E., et al. (2016). Three climatic cycles recorded in a loess-palaeosol sequence at Semlac (Romania) – Implications for dust accumulation in south-eastern Europe. *Quat. Sci. Rev.* 154, 130–142. doi:10.1016/j.quascirev.2016.11.002.